

Molecular dynamics simulation of the order-disorder phase transition in solid NaNO_2

Wei-Guo Yin,^{1,*} Chun-Gang Duan,¹ W. N. Mei,¹

Jianjun Liu,^{1,2} R. W. Smith,¹ and J. R. Hardy²

¹*Department of Physics, University of Nebraska, Omaha, NE 68182*

²*Department of Physics and Center for Electro-Optics,
University of Nebraska, Lincoln, NE 68588*

(Dated: November 16, 2018)

Abstract

We present molecular dynamics simulations of solid NaNO_2 using pair potentials with the rigid-ion model. The crystal potential surface is calculated by using an *a priori* method which integrates the *ab initio* calculations with the Gordon-Kim electron gas theory. This approach is carefully examined by using different population analysis methods and comparing the intermolecular interactions resulting from this approach with those from the *ab initio* Hartree-Fock calculations. Our numerics shows that the ferroelectric-paraelectric phase transition in solid NaNO_2 is triggered by rotation of the nitrite ions around the crystallographical c axis, in agreement with recent X-ray experiments [Gohda *et al.*, Phys. Rev. B **63**, 14101 (2000)]. The crystal-field effects on the nitrite ion are also addressed. Remarkable internal charge-transfer effect is found.

PACS numbers: 64.60.Cn, 61.43.Bn, 64.70.Pf

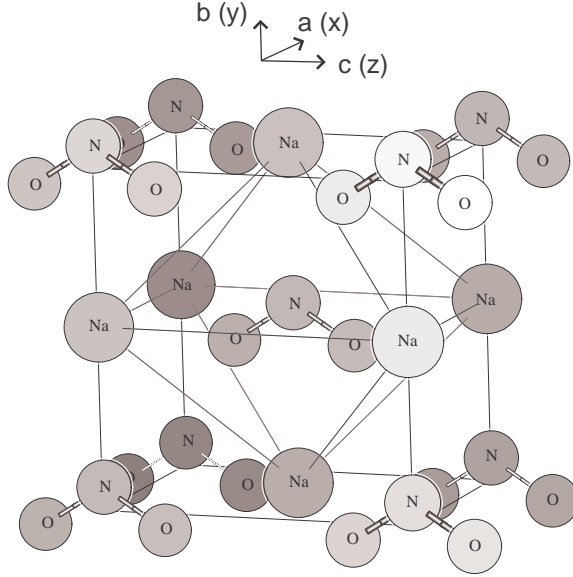


FIG. 1: Crystal structure of NaNO_2 in the ferroelectric phase.

I. INTRODUCTION

Sodium nitrite is a ferroelectric at room temperature. It has the orthorhombic structure, space group $C_{2v}^{20} - Im2m$, with the dipole vector of the V-shaped nitrite anions aligned parallel to the crystallographic b direction, as shown in Fig. 1. The ferroelectric-paraelectric phase transition takes place at about 437 K, where the high temperature phase is orthorhombic, space group $D_{2h}^{25} - Immm$, with the dipoles disordered with respect to the b axis. In a narrow temperature range from 435.5 K to 437 K, there exists an incommensurate antiferroelectric phase. The melting temperature is 550 K. Distinguished from displacive ferroelectrics in which the ferroelectric transition is driven by soft phonon modes, NaNO_2 offers a model system for research of the order-disorder structural phase transition and any associated ferroelectric instability.^{1,2,3}

Extensive experimental work on NaNO_2 has been devoted to probing the mechanism of the NO_2^- polarization reversal that triggers the order-disorder transition. The majority of studies support the c -axis rotation model, but there were also results favoring the a -axis rotation model.⁴ Recently, refined X-ray studies over a wide temperature range reinforced the c -axis rotation model.^{4,5} On the theoretical side, the microscopic model calculations done by Ehrhardt and Michel supported the c -axis rotation mechanism,⁶ whereas mixed double rota-

tions around the a -axis and the c -axis was suggested by Kinase and Takahashi.⁷ It has long been desirable to apply computer molecular dynamics (MD) simulations to NaNO_2 in order to achieve unambiguous understanding of the polarization reversal mechanism. Earlier MD simulations with empirical Born-Mayer pair potentials detected the c -axis rotation in above-room-temperature NaNO_2 .^{8,9,10} Unfortunately, the low-temperature structure produced by those simulations was antiferroelectric and apparently disagreed with the experimental observations.

Lu and Hardy pointed out that the overall phase behavior of NaNO_2 could be simulated by using an *a priori* approach to construct the crystal potential surface (PES).¹¹ The Lu-Hardy (LH) approach was originally designed to deal with molecular crystals such as K_2SeO_4 , where exists a mix of bonding types, that is, the intermolecular interactions are mostly ionic, but the constituent atoms in a molecule (SeO_4^{2-} in K_2SeO_4) bond covalently. In the LH approach, the intra-molecule interactions were treated by applying the *ab initio* self-consistent field method to the gas-phase molecules, while the intermolecular pair potentials were computed within the Gordon-Kim (GK) electron gas theory.¹² The crux of their application of the GK theory is how to partition the *ab initio* molecular charge density between the constituent atoms. Since there is no unique way to separate the charge density of a highly covalently bonded molecule, Lu and Hardy suggested equal separation in a spirit similar to the Mulliken population analysis (MPA). By using this atomic-level method, we could successfully describe the phase transitions in fluoroperovskites,¹³ and ionic crystals with polyatomic molecules including SeO_4^{2-} ,¹⁴ ClO_4^- ,¹⁵ SO_4^{2-} ,¹⁶ SiO_4^{4-} ,¹⁷ and NO_3^- .^{18,19,20} Note that the MPA happens to preserve the (zero) dipole moment of these molecules.

However, several problems appear when we moved on to deal with NaNO_2 where the NO_2^- radical has nonzero dipole moment and stronger chemical bonding. First, it is well known that the MPA, while certainly the most widely employed, is also somewhat arbitrary and the most criticized.²¹ In particular, the MPA overestimates the dipole moment of the free NO_2^- ion by about 120%. Other difficulties involved the free-ion approximation. Unlike in monatomic ionic crystals, there may exist considerable *internal* charge-transfer effects in molecular ionic crystals. Electronic band structure calculations²² indicated that within a nitrite entity, the nitrogen atom and two oxygen atoms bond covalently, leading to high charge transferability between these constituent atoms. Therefore, in solid NaNO_2 the NO_2^- group will feel different crystal-field environments as it rotates and responds by redistributing

the charge density among its three constituent atoms.

Our goals in this paper are twofold. First, we show that our atomistic level simulation methods involving pair potentials with the rigid-ion model is capable of correctly describing the phase behavior of NaNO_2 . Second, we systematically examine the LH approach to understand the reason why it works so well in molecular ionic crystal systems by the following steps: (i) we develop another population analysis method that preserves the molecular dipole moment by directly fitting the *ab initio* charge density of a molecule; (ii) we carry out *ab initio* Hartree-Fock (HF) calculations of the intermolecular interactions and find that the pair potentials from the rigid-ion model can correctly reproduce the *ab initio* results; (iii) we investigate the crystal-field effects on the NO_2^- ion by embedding the ion (and its first shell of neighbors) in a lattice of point charges and find a remarkable internal charge-transfer effect.²³ Several MD simulations based on these modifications of the LH approach are also performed. The ferroelectric-paraelectric transition triggered by the *c*-axis rotation of the nitrite ions is observed in all versions of the LH approach. However, the transition temperatures predicted by these simulations are lower than the experimental values. Furthermore, the transition temperatures obtained from the original version are higher than those predicted by modified versions and closer to the experimental values. After careful examination, we notice that in the LH approach, the NO_2^- dipole moments were generally overestimated by about 120%, which reinforces the ground state. This implies that the crystal structure of NaNO_2 is stabilized by the anion polarization effects. Thus, we conclude polarization effects are particularly important for the quantitative study of NaNO_2 .

This paper is organized as follows. Section II describes the method we used to obtain the intermolecular interactions. Section III analyzes the resulting intermolecular potentials in comparison with those obtained from *ab initio* calculations. Section IV presents the results of our MD simulations. The crystal-field effects on NO_2^- are discussed in Section V. Concluding remarks are made in Section VI.

II. INTERMOLECULAR INTERACTIONS

Our MD simulation technique method originates from the GK model for simple ionic crystals such as alkali halides, assuming that (molecular) ions in a crystal environment may be described as free ions.^{24,25,26} Then it was extended to deal with molecular ionic crystals

like K_2SeO_4 , in which strong intramolecular covalency exists.^{12,14} The main idea is that the molecular ion (SeO_4^- in K_2SeO_4) is treated as a single entity, and intramolecular and intermolecular interactions are treated separately: first we perform *ab initio* quantum chemistry calculations for the whole molecular ion, to obtain the optimized structure, the force constants, and the whole electron density $\rho(\mathbf{r})$. The intramolecular interactions are described by force constants within the harmonic approximation. As for the intermolecular interactions, we have to carry out electron population analysis to separate $\rho(\mathbf{r})$ onto each individual atom in the molecular ion, then use the Gordon-Kim electron gas model to calculate the intermolecular pair potentials. This approach provides a parameter-free description for the crystal potential-energy surfaces, which allow structural relaxation, MD simulation, and lattice dynamics calculations.

In calculating the intermolecular forces, there are three major approximations as discussed in the following:

(1) We assume that the geometries and electronic densities of the separate ions remain unchanged once they have been obtained under given circumstance, such as in the equilibrium state of the gas or crystal phases. This approximation is the fundamental basis for the GK electron gas theory. General speaking, we found that in an ionic crystal there is no strong chemical bond between ions, hence this approximation is reasonable.

(2) When dealing with the intermolecular interaction, we assume that the charge density of a rigid ion can be separated into its atomic constituents.

(3) We assume that the crystal potential energy is composed of the intermolecular and intramolecular interaction, where the intramolecular interaction is expressed in terms of force fields and the intermolecular interaction is a sum of interatomic pair potentials.

Atomistic level simulations utilizing pair potentials and the rigid-ion model have great success in describing many ionic systems.²⁷ We showed that this scheme can correctly describe the phase transition behaviors of alkali halide fluoperovskites,¹³ and molecular crystals with tetrahedral^{12,14,15,16,17} and equilateral triangular^{18,19,20} radicals. However, for NaNO_2 in which NO_2^- has only a two fold symmetrical axis, the results were less satisfactory.¹¹ Note that the mean HF polarizability of NO_2^- , 14.156 (atomic units), calculated with the D95* basis,²⁸ is much higher than that of Na^+ , 0.343 (atomic units), calculated with the 6-31* basis. Therefore, in solid NaNO_2 , the rotation of NO_2^- in the crystal field will induce charge redistribution within the molecule. Hence this dynamic effect may invalidate the rigid ion

approximation. In this paper we shall perform HF calculations for various geometries to verify this scenario.

A. Pairwise additive approximation

In the GK model, we evaluate the interaction between two molecules based on the electron density,²⁹ which is approximated as the sum of component densities taken from HF calculations. That is, if ρ_A and ρ_B are the component densities, then the total density is $\rho_{AB} = \rho_A + \rho_B$. Whereas, interaction potential is computed as the sum of four terms: Coulombic, kinetic, exchange, and correlation energies which are expressed in terms of the charge densities.

Therefore, suppose the A and B molecules are made up of M and N atoms, respectively, then the Coulombic interaction between them is

$$V_C = \int \int d\mathbf{r}_1 d\mathbf{r}_2 \frac{\rho_A(\mathbf{r}_1)\rho_B(\mathbf{r}_2)}{|\mathbf{r}_1 - \mathbf{r}_2|} - \sum_{i=1}^M Z_{A,i} \int d\mathbf{r}_2 \frac{\rho_B(\mathbf{r}_2)}{|\mathbf{r}_2 - \mathbf{R}_{A,i}|} \\ - \sum_{j=1}^N Z_{B,j} \int d\mathbf{r}_1 \frac{\rho_A(\mathbf{r}_1)}{|\mathbf{r}_1 - \mathbf{R}_{B,j}|} + \sum_{i=1}^M \sum_{j=1}^N \frac{Z_{A,i}Z_{B,j}}{|\mathbf{R}_{A,i} - \mathbf{R}_{B,j}|}, \quad (1)$$

where $Z_{A,i}$, $Z_{B,j}$, $\mathbf{R}_{A,i}$ and $\mathbf{R}_{B,j}$ are the nuclear charges and coordinations of the i -th atom in the A molecule and j -th atom in the B molecule, respectively. This potential energy can be split into two parts: first the long-range part,

$$V_C^l = \sum_{i=1}^M \sum_{j=1}^N \frac{[Z_{A,i} - \int \rho_A(\mathbf{r}_1) d\mathbf{r}_1][Z_{B,j} - \int \rho_B(\mathbf{r}_2) d\mathbf{r}_2]}{|\mathbf{R}_{A,i} - \mathbf{R}_{B,j}|}, \quad (2)$$

and the short-range part

$$V_C^s = V_C - V_C^l. \quad (3)$$

Eq. (2) is essentially the electrostatic interaction energy when the charge densities of the molecules are distributed as point charges on the constituent atoms, which is known as the Madelung potential energy.

The non-Coulombic energy terms are expressed in the uniform electron gas formula,

$$V_i = \int d\mathbf{r} [\rho_{AB}(\mathbf{r})\epsilon_i(\rho_{AB}) - \rho_A(\mathbf{r})\epsilon_i(\rho_A) - \rho_B(\mathbf{r})\epsilon_i(\rho_B)], \quad (4)$$

where $\epsilon_i(\rho)$ is one of the energy functionals for the kinetic, exchange, and correlation interactions.²⁹ Note that Eq. (4) is not composed of pair potentials. In order to obtain the effective pairwise potentials, we approximate Eq. (4) using

$$V_i \simeq \sum_{m \in A} \sum_{n \in B} \int d\mathbf{r} [\rho_{mn}(\mathbf{r}) \epsilon_i(\rho_{mn}) - \rho_m(\mathbf{r}) \epsilon_i(\rho_m) - \rho_n(\mathbf{r}) \epsilon_i(\rho_n)], \quad (5)$$

where $\rho_{mn} = \rho_m + \rho_n$. ρ_m and ρ_n are the charge densities of individual atoms in the A and B molecules, respectively, which are obtained by a population analysis as described in the next subsection.

Even though the non-Coulombic forces as determined by Eq. (4) are not strictly additive, the above approximation appears to be adequate except at very short distances. As pointed out by Waldman and Gordon,³⁰ the main reason as to why this approximation is valid is because the Coulombic force, the largest contribution to the potentials, is additive. Based on our calculations, we find additivity of V_i holds only to within about 50%; however, the overlap contribution to the electrostatic energy dominates V_i and renders additivity to within 10%. One final remark is in order, for the sake of simplifying the two-electron integral in Eq. (1), the charge densities, ρ_m and ρ_n , are taken as its spherical average. As a result, the Coulombic interaction is not exactly evaluated. Nevertheless, as we shall show in Figs. 2 and 3, this error is compensated by those due to the pairwise additive approximation.

To summarize this subsection, we demonstrated that it is possible to analytically express the intermolecular potentials $V_C^l + V_C^s + V_i$ using Eqs. (2), (3) and (5) once the charge density of each individual atom is obtained by an electronic population analysis. In the next subsection, we shall present further analysis on the charge density.

B. Electronic Population Analysis

In this subsection, we discuss the ways to separate the electron density $\rho(\mathbf{r})$ of a molecule into its atomic constituents. Suppose the molecule consists of M atoms, then the wave function of the molecule $\psi(\mathbf{r})$ can be written as a linear superposition of atomic wave functions $\varphi(\mathbf{r} - \mathbf{R}_i)$, $i = 1, 2, \dots, M$, centered at each atom,

$$\psi(\mathbf{r}) = \sum_{i=1}^M \varphi(\mathbf{r} - \mathbf{R}_i). \quad (6)$$

In turn, the atomic wave functions $\varphi(\mathbf{r} - \mathbf{R}_i)$ can be written as a linear superposition of the basis functions χ_l

$$\varphi(\mathbf{r} - \mathbf{R}_i) = \sum_l c_{il} \chi_l(\mathbf{r} - \mathbf{R}_i). \quad (7)$$

where $\{\chi_l(\mathbf{r} - \mathbf{R}_i)\}$ are usually the gaussian basis functions, and the coefficients c_{il} can be obtained from the variational method.

Then the electronic density of the molecule is,

$$\rho(\mathbf{r}) = |\psi(\mathbf{r})|^2 = \sum_{ijkl} d_{ik,jl} \chi_k(\mathbf{r} - \mathbf{R}_i) \chi_l(\mathbf{r} - \mathbf{R}_j), \quad (8)$$

where $d_{ik,jl} = 2c_{ik}c_{jl}$, which can be divided into two parts, namely the *net* ($i = j$) and *overlap* ($i \neq j$) populations. The latter cannot be ignored in the presence of strong intramolecular covalency. Therefore, separating $\rho(\mathbf{r})$ into its atomic constituents is to split the overlap population. However, the way to achieve that is not unique. For example, we can introduce a set of weights w_{ijkl} due to different criteria such that

$$\begin{aligned} \tilde{d}_{ik,ik} &= d_{ik,ik} + \sum_{j \neq i,l} w_{ijkl} d_{ik,jl} \int \chi_k(\mathbf{r} - \mathbf{R}_i) \chi_l(\mathbf{r} - \mathbf{R}_j) d\mathbf{r}, \\ \tilde{d}_{jl,jl} &= d_{jl,jl} + \sum_{i \neq j,k} (1 - w_{ijkl}) d_{ik,jl} \int \chi_k(\mathbf{r} - \mathbf{R}_i) \chi_l(\mathbf{r} - \mathbf{R}_j) d\mathbf{r}, \\ \tilde{d}_{ik,il} &= d_{ik,il}, \end{aligned} \quad (9)$$

then we can rewrite Eq. (8) as following

$$\rho(\mathbf{r}) \simeq \sum_i \rho_i(\mathbf{r}) = \sum_{ikl} \tilde{d}_{ik,jl} \chi_k(\mathbf{r} - \mathbf{R}_i) \chi_l(\mathbf{r} - \mathbf{R}_i), \quad (10)$$

where $\rho_i(\mathbf{r})$ is the atomic density of atom i .

In our previous studies, the overlap electronic density is equally separated, i.e., $w_{ijkl} = 1/2$ in Eq. (9), similar to the Mulliken population analysis (MPA).^{11,12,17,18,31} In Table I, we present the electronic multipole moments of SnCl_6^{2-} , ScF_6^{3-} , SiO_4^{4-} , SeO_4^{2-} , SO_4^{2-} , ClO_4^- , CO_3^{2-} , and NO_3^- calculated from using the MPA, and compare them with the *ab initio* values. We note that for these symmetrical molecules, the MPA preserves total charge and zero dipole moment. However, for a molecular ion like V-shaped NO_2^- or linear CN^- , the Mulliken population seems inadequate. Given total charge and the dipole moment, 0.26 a.u., of NO_2^- obtained from the *ab initio* calculations (Table I), a population analysis which

TABLE I: Electronic multipole moments of molecule (AB_n) calculated from the Mulliken population analysis. The *ab initio* values are shown in parentheses. All quantities are in atomic units.

AB_n^a	μ_z^b	ϑ_{zz}	Ω_{zzz}	Φ_{zzzz}
CN ⁻	0.14 (0.17)	-27.35 (-29.41)	7.99 (10.68)	-143 (-166)
NO ₂ ⁻	0.57 (0.26)	-19.64 (-21.64)	-2.60 (-5.87)	-60 (-76)
NO ₃ ⁻	0 (0)	-15 (-16)	0 (0)	-38 (-41)
CO ₃ ²⁻	0 (0)	-17 (-17)	0 (0)	-48 (-48)
ClO ₄ ⁻	0 (0)	-111 (-111)	0 (0)	-548 (-548)
SO ₄ ²⁻	0 (0)	-119 (-120)	0 (0)	-620 (-627)
SeO ₄ ²⁻	0 (0)	-143 (-143)	0 (0)	-823 (-816)
SiO ₄ ⁴⁻	0 (0)	-157 (-158)	0 (0)	-1011 (-1019)
ScF ₆ ³⁻	0 (0)	-319 (-318)	0 (0)	-5112 (-5071)
SnCl ₆ ²⁻	0 (0)	-845 (-844)	0 (0)	-19834 (-19668)

^aIn the HF calculations, basis set D95* were used for AB and AB_2 , 6-31G* for AB_3 and AB_4 , and 3-21G* for AB_6 .

^bThe electrostatic moments μ (dipole), ϑ (quadrupole), Ω (octapole), and Φ (hexadecapole) refer to the center of mass of the molecule with the standard orientation defined in GAUSSIAN 98 (Ref. 28).

preserves these vales would give rise to $-0.092e$ on N and $-0.454e$ on O. Whereas, using the MPA ($w_{ijkl} = 1/2$), the charges on the N and O atoms are $0.1624e$ and $-0.5812e$, respectively, which renders the dipole moment 0.57 atomic unit, overestimated by 120%.

Therefore, it is desirable to determine w_{ijkl} in such a way that the calculated multipole moments of the molecule are consistent with the *ab initio* values. One possible way is to evaluate w_{ijkl} by fitting the *ab initio* charge density, as shown in Eqs. (9) and (10), with the values of multipole moments as constraints. An alternative way is to directly fit the charge density, Eq. (10), with $\tilde{d}_{ik,jl}$ being the parameters and $\chi_k(\mathbf{r}-\mathbf{R}_i)\chi_l(\mathbf{r}-\mathbf{R}_i)$ being the dependent variables. To simplify the computation, only the radial parts of $\chi_k(\mathbf{r}-\mathbf{R}_i)\chi_l(\mathbf{r}-\mathbf{R}_i)$ were kept. This fitting population analysis (FPA) is similar to that proposed by Parker and his co-workers as an alternative implementation of the GK model.³²

C. Free ion and intramolecular interactions

GAUSSIAN 98 program package²⁸ is employed to obtain the self-consistent solutions to the Hartree-Fock-Roothan equations. The atomic orbital basis sets used are a double-zeta basis with polarization functions (D95*) for the nitrogen and oxygen atoms. It was shown that this choice of basis set could give a good description of free NO_2^- .³³ As for the sodium atoms, we used both the standard 6-31G* basis and the Slater-type orbitals for Na^+ taken from the Clementi and Roetti table,³⁴ it turned out the difference between them is small.

We first consider the free ion case and will discuss the in-crystal ions in Section IV. The molecular geometry of NO_2^- can be described by internal coordinates $(R_{\text{NO}_1}, R_{\text{NO}_2}, \theta_{\text{ONO}})$ where R_{NO_1} and R_{NO_2} are the lengths of the two N-O bonds, respectively, and θ_{ONO} is the angle formed by the two N-O bonds. The minimum energy geometry of NO_2^- using our basis yields $R_{\text{NO}}^0 = 1.233 \text{ \AA}$ and $\theta_{\text{ONO}}^0 = 116.6^\circ$. These structural parameters are comparable to the experimental geometry of NO_2^- in the ferroelectric phase of NaNO_2 ,³⁵ in which $R_{\text{NO}}^0 = 1.236 \text{ \AA}$ and $\theta_{\text{ONO}}^0 = 115.4^\circ$. The internal vibration frequencies of the NO_2^- group are then calculated at the optimized geometry. Note that the lowest vibration frequency (1192 K) of NO_2^- is considerably higher than the highest libration frequency (318 K) obtained from Raman spectroscopy³⁶ as well as the order-disorder transition temperature (437 K). Therefore, it is justified to treat the internal motion of the nuclei in the NO_2^- group within the harmonic approximation, or even as a rigid rotor. To further support this argument, we found that only small changes in the geometry of NO_2^- were observed in the high temperature paraelectric phase ($R_{\text{NO}}^0 = 1.239 \text{ \AA}$ and $\theta_{\text{ONO}}^0 = 114.5^\circ$).⁵

The intramolecular interactions are then represented by the following force field obtained from frequency analysis in GAUSSIAN 98:²⁸

$$U = U_0 + \frac{1}{2}k_{\text{NO}}[(R_{\text{NO}_1} - R_{\text{NO}}^0)^2 + (R_{\text{NO}_2} - R_{\text{NO}}^0)^2] + \frac{1}{2}k_{\text{ONO}}(\theta_{\text{ONO}} - \theta_{\text{ONO}}^0)^2 + k_2(R_{\text{NO}_1} - R_{\text{NO}}^0)(R_{\text{NO}_2} - R_{\text{NO}}^0) + k_3(R_{\text{NO}_1} + R_{\text{NO}_2} - 2R_{\text{NO}}^0)(\theta_{\text{ONO}} - \theta_{\text{ONO}}^0) \quad (11)$$

where $U_0 = -204.121$, $R_{\text{NO}}^0 = 2.330$, $\theta_{\text{ONO}}^0 = 2.036$, $k_{\text{NO}} = 0.728$, $k_{\text{ONO}} = 0.677$, $k_2 = 0.174$, $k_3 = 0.066$ in atomic units.

Note that the polarizability of NO_2^- at its optimized geometry is highly anisotropic, that is, with $\alpha_{xx} = 7.820$, $\alpha_{yy} = 10.823$, $\alpha_{zz} = 23.825$ in atomic units (see Fig. 1 for coordinate convention). Thus, one would expect this polarization to seriously affect the intermolecular

pair potentials, and thus renders the rigid-ion approximation in question. Nevertheless, after extensive *ab initio* HF calculations with various configurations, which will be presented in the next subsection, we find that the intermolecular potentials for the $\text{NO}_2^-:\text{Na}^+$ and $\text{NO}_2^-:\text{NO}_2^-$ dimers can still be correctly reproduced.

III. INTERMOLECULAR POTENTIALS

We scan the potential energy surface of $\text{NO}_2^-:\text{Na}^+$ and $\text{NO}_2^-:\text{NO}_2^-$ obtained from the Hartree-Fock method. In these calculations, the geometrical variables of NO_2^- are frozen at their equilibrium values, since we showed previously that the NO_2^- group in NaNO_2 could be treated as a rigid rotor. However in the *ab initio* HF calculations, the electronic structure is allowed to vary in order to minimize the total energy, thus the electronic polarization effects are included.

In our calculations of intermolecular interactions, one NO_2^- is fixed with its center of mass being the origin of the coordinate system, the dipole vector pointing to the y axis and the O-O line being aligned parallel to the z axis (see Fig. 1). Then, Cartesian coordinates (x, y, z) are the position of Na^+ or the center of mass of another NO_2^- . To describe the orientation of the NO_2^- molecule at (x, y, z) , we use the angles α and β of the dipole moment vector of the NO_2^- molecule and an angle γ involving the rotation of NO_2^- around its dipole vector.

In order to study the effects of the different partition schemes, mentioned in Section IIB, on the pair potentials, we performed three different calculations, namely (i) MPA with pair potentials [Eq. (5)], (ii) FPA with pair potentials, (iii) FPA with non-pair potentials as shown in Eq. (4). We shall refer them as models I, II, and III, respectively, from now on. Recall that model I overestimates the dipole moment of NO_2^- as mentioned in Section IIB. Furthermore, we shall show in the following that the electronic polarization effect could be revealed from examining the differences between model I and II, while the errors due to the pairwise additive approximation employed by the GK model could be analyzed from the differences between model II and III.

In Figs. 2 and 3, we compare the pair potentials obtained from these models and those from the *ab initio* HF calculations. In Fig. 2 we show the results for the $\text{NO}_2^-:\text{Na}^+$ dimer: we find that in both models I and II, the overall shapes of the GK potentials as a function of molecular separation are in agreement with the *ab initio* results, particularly in Fig. 2(d). On

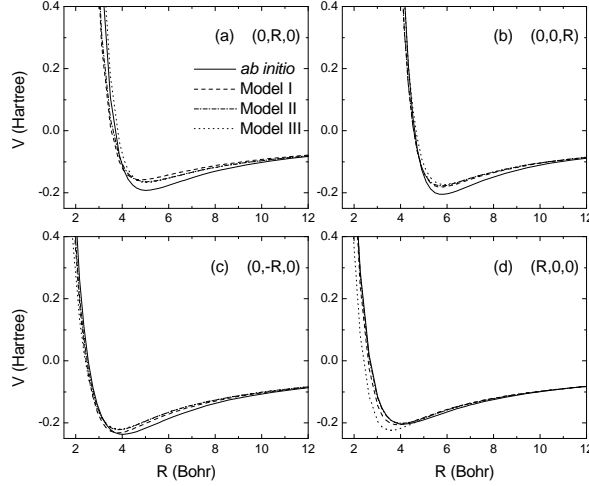


FIG. 2: NO_2^- - Na^+ intermolecular potential energy curves as a function of R for various configurations: $(0, R, 0)$, $(R, 0, 0)$, $(0, -R, 0)$, and $(0, 0, R)$, where (x, y, z) is the location of Na^+ . Different lines represent the *ab initio* HF model (solid), model I (dashed), model II (dotted), and model III (dashed and dotted).

the other hand, the electronic polarization effect also manifests itself in Fig. 2 based on the following two observations. First, notice Figs. 2(b) and 2(d), models I and II fit the *ab initio* results through the entire range in $(R, 0, 0)$, whereas in $(0, 0, R)$ models I and II overestimate the potentials when $5 < R < 8$. We attribute that to the anisotropic polarizability of NO_2^- ($\alpha_{xx} < \alpha_{yy} < \alpha_{zz}$), thus the electronic cloud of NO_2^- is most unlikely to be polarized along the $(R, 0, 0)$ direction, along which the polarization is the weakest, rather than the $(0, 0, R)$ direction. Second, in Fig. 2(a), $(0, R, 0)$, the minimum potential energy in model II is closer to the *ab initio* values than model I, whereas in $(0, -R, 0)$, where Na^+ is located below NO_2^- , we found the situation reversed. To understand this, we observe that in the $(0, R, 0)$ configuration, Na^+ is closer to N than O, thus in the *ab initio* calculations the electrons were attracted toward the N atom and thus led to a smaller dipole moment. Therefore, model II, which produced smaller dipole moment than model I, tends to get closer to the HF results. Obviously, the results will be opposite if the situation is reversed.

Among the four different configurations, Figs. 2(a) through 2(d), and methods except model III, the lowest NO_2^- - Na^+ potential energy takes place at $(0, -R, 0)$, which will be shown later to give rise to the lowest energy structure of NaNO_2 . Both models II and III use FPA, the only difference between them is that model II employs the pair potentials. It seems

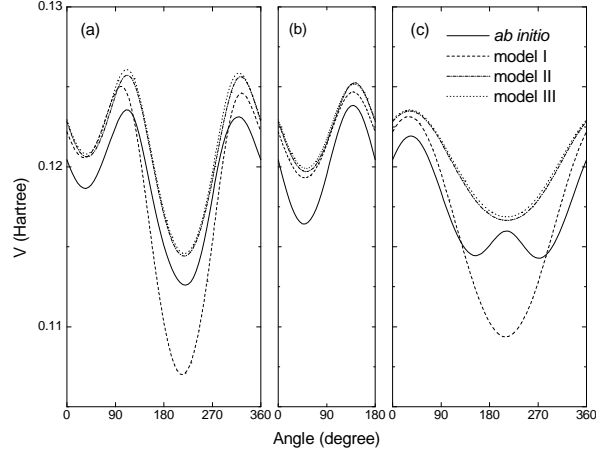


FIG. 3: NO_2^- - NO_2^- intermolecular potential energy curves as a function of rotation angle. The NO_2^- molecules are initially in parallel alignment at separation (1.82 Å, 2.83 Å, 2.69 Å) and then one of them rotates around one of the (a) x , (b) y and (c) z axes through its center of mass.

that in model II the errors caused by the pairwise additive approximation is compensated by the errors due to FPA.

Similarly, we show in Fig. 3 the NO_2^- - NO_2^- intermolecular potentials using the same four methods. The configurations are chosen as follows: the two NO_2^- molecules are initially parallel at their experimental low-temperature separation (1.82 Å, 2.83 Å, 2.69 Å) and then one of them rotates around each of the x , y , z axes through its center of mass, as shown in Figs. 3(a) through 3(c). The results of models I-III agree reasonably well with the *ab initio* calculations. On closer examination, Models II and III fit better to the *ab initio* results than I. We believe this is due to the fact that the two nitrite ions are separated so far that the main contribution to the intermolecular potential is mostly electrostatic. Based on the experience acquired in Section IIB, FPA usually gives a better description of the rigid NO_2^- molecule than MPA, hence the results obtained from models II and III which employ the FPA are considerably better. In addition, the short range interaction is also small, thus the difference between model II and III is rather small.

Summarizing this section, in spite of the presence of electronic polarization when two molecules are brought closer, the intermolecular potentials for the $\text{NO}_2^-:\text{Na}^+$ and $\text{NO}_2^-:\text{NO}_2^-$ dimers could be correctly reproduced using models I and II. Furthermore, model II appears to give better description of NO_2^- than model I as shown in Fig. 3, particularly Figs. 3(a)

TABLE II: Experimental and theoretical structural parameters for the $Im2m$ phase (III) of $NaNO_2$. Lattice constants are given in Å.

Parameters	Experiment ^a	Model I	Model II	Model III
a	3.5180	3.3889	3.5013	3.7353
b	5.5350	5.4542	5.5485	5.4257
c	5.3820	4.9254	4.8403	4.9669
y/b of N (2a)	0.5437	0.0498	0.0433	0.0586
y/b of Na (2a)	0.0781	0.5537	0.5492	0.5437
y/b of O (4d)	-0.0443	-0.0704	-0.0740	-0.0610
z/c of O (4d)	0.1962	0.2111	0.2151	0.2098

^aFrom X-ray diffraction experiments at 120 K, see Ref. 37.

and 3(c).

IV. MOLECULAR DYNAMICS SIMULATIONS

After the potential energy surface for $NaNO_2$ has been obtained, we are prepared to undertake MD simulations. Long-range Coulombic interaction in the crystal is represented by electrostatic interaction among point charges calculated from the population analysis, while each of the short-range pair potentials are fitted by using an exponential-polynomial function accurate within 0.1%.¹⁸ In the following description, the x , y , z directions correspond to the crystallographic a , b , c directions of $NaNO_2$, respectively, see Fig. 1.

A. Lattice relaxation

Before we proceed with the molecular dynamics simulations, we perform lattice relaxation for the ferroelectric structure of $NaNO_2$ both with and without the $Im2m$ space group symmetry constraints. This relaxation procedure provides the crystal structure with zero force on each atom, that is an energy extremum; it also produces a test to the PES because the resultant structures have to agree reasonably with the experimental data for further simulations to be reliable. We perform both static and dynamic relaxations: the static

one is an application of the Newton-Raphson algorithm and usually results in finding a local minimum of the energy, and the dynamic one is a simulated annealing calculation for overcoming that limitation. We start the static lattice relaxation with the experimental parameters. In Table II we present the lattice and basis parameters deduced from the experiments and static relaxation. In all cases, the static relaxation produced essentially the same structure that strongly resembles the experimental structure. Most of the lattice constants in the relaxed structure are shorter than the experimental values (by 3.7%, 1.5%, and 8.5% for a , b , and c , respectively, in model I, and by 0.5%, -2.4%, and 10% for a , b , and c , respectively, in model II). Hence the calculated volume is smaller than the experimental one by 13% for model I and 10% for model II, a common feature for simulations using the GK model, which will be addressed in more detail in the next subsection.

Next, we go on to relax the statically relaxed crystal structure to zero temperature using a simulated annealing algorithm, in which the amount of kinetic energy in the molecules slowly decreases over the course of the simulation. We find that the (zero temperature) ground states in models I and II are close to the statically relaxed structures, whereas there are substantial changes taking place in model III. By monitoring the orientations of the nitrite ions, we find that the ground structure in model III, still orthorhombic with $a = 3.90494$ Å, $b = 4.8441$ Å, and $c = 5.0770$ Å, is ferroelectric with the dipole moments of NO_2^- aligned along the a axis rather than the experimental b axis. So we conclude that the PES given by models III did not reflect reality. This concurs with the previous discussion (Section III) on the intermolecular potentials. In the following we use only models I and II to simulate the phase transition in NaNO_2 .

B. MD simulations

Using the isenthalpic, isobaric ensemble, our MD simulation is started with a zero-temperature zero-pressure orthorhombic cell ($4a \times 4b \times 4c$), consisting of 512 atoms. Periodic boundary conditions are imposed to simulate an infinite crystal. The MD calculations are carried out in the Parrinello-Rahman scheme³⁸ which allows both the volume and the shape of the MD cell to vary with time. The calculation of the energies and forces was handled by the Ewald method. A time step of 0.002 ps was used to integrate the equations of motion. In our heating runs, we raise the temperature of the sample in stages, 20 K each time, up

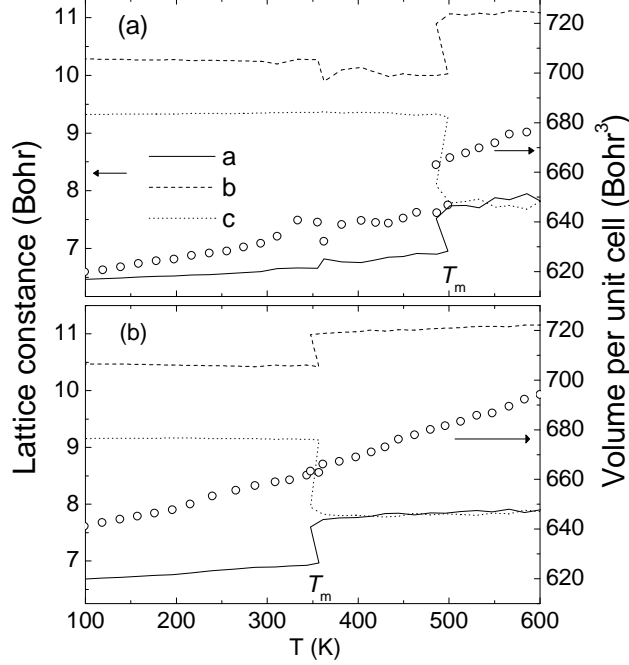


FIG. 4: Temperature variation of lattice constants a , b , c (solid, dashed, dotted lines, respectively; left scale) and volume of the unit cell (open circles; right scale) for (a) model I and (b) model II.

to 1000 K. At each stage, the first 2000 time steps were employed to equilibrate the system, then 10000 time steps were collected for subsequent statistical analysis. Since our simulations employ periodic boundary conditions, we cannot distinguish the incommensurate structure (i.e., phase II of solid NaNO_2).

In Figs. 4 through 7, we demonstrate that as the MD cell is heated, it undergoes two phase transitions: in the first one, the system retains its orthorhombic structure with a change of space group from $Im2m$ to $Immm$, in agreement with the experiments. The critical temperature T_C is around 400 K for model I and 313 K for model II, respectively. In the second transition, the crystal structure violently changes from orthorhombic to tetragonal at temperature (T_m) which is around 500 K for model I and 350 K for model II, as shown in Fig. 4. However, we argue that the crystal has already melted before this type of transition could be observed in reality.

To investigate the mechanism of the polarization reversal of NO_2^- , we monitor the crystal polarization and display the results in Fig. 5. Let the dipole moment of anion i be \mathbf{m}_i and the quadrupole moment be ϑ_i calculated by using the point charges on the N and O atoms. Then the mean dipole moment per anion at temperature T is $\mathbf{M}(T) = \sum_i \langle \mathbf{m}_i \rangle / N$ where $N = 128$

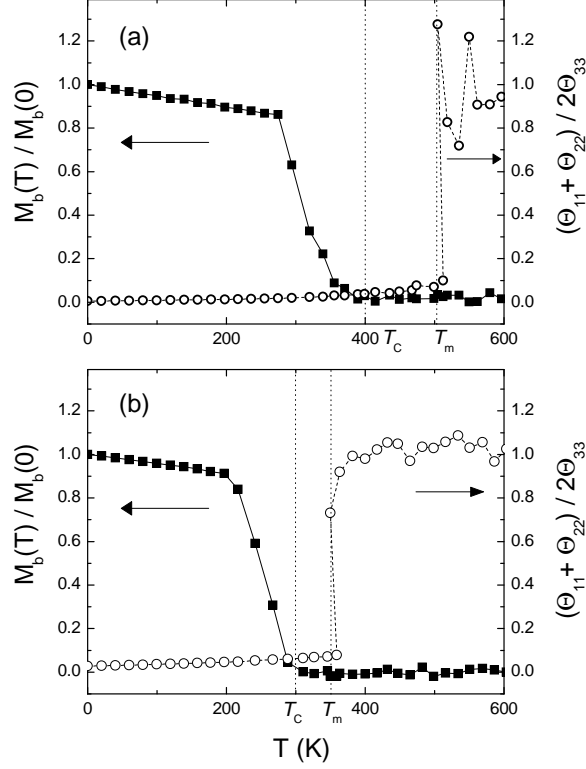


FIG. 5: Mean dipole moment $M_b(T)$ and quadrupole moment Θ of the whole NaNO_2 crystal as a function of temperature for the MD runs for (a) model I and (b) model II.

is the number of NO_2^- in the MD cell and the brackets denote an average over the MD run. In addition, we define the antiferroelectric polarization as $\mathbf{Q} = \sum_i \exp(-\pi \cdot \mathbf{R}_i) \langle \mathbf{m}_i \rangle / N$ where $\pi = (\pi, \pi, \pi)$ and \mathbf{R}_i is the lattice vectors associated with the i -th ion. Within our statistical uncertainty we find over all temperature range $M_x = M_z = \mathbf{Q} = 0$, while $M_y(T < T_C) > 0$ and $M_y(T > T_C) = 0$. This fact confirms that the transition taking place at T_C is the ferroelectric-paraelectric phase transition. Furthermore, we calculated the mean quadrupole moment $\Theta = \sum_i \langle \vartheta_i \rangle / N$. When the dipole vector of a NO_2^- is aligned along the b axis, $\vartheta_{xx} \simeq 0.00$, $\vartheta_{yy} \simeq -0.04$, $\vartheta_{zz} \simeq -4.49$ for model I and $\vartheta_{xx} \simeq 0.00$, $\vartheta_{yy} \simeq -0.20$, $\vartheta_{zz} \simeq -3.52$ for model II; thus $(\Theta_{xx} + \Theta_{yy})/2\Theta_{zz} \ll 1$. This relation holds as the NO_2^- ion rotates around the c axis; nevertheless, one would expect $(\Theta_{xx} + \Theta_{yy})/2\Theta_{zz} = 1$ when the NO_2^- ion rotates without directional preference. The fact that $(\Theta_{xx} + \Theta_{yy})/2\Theta_{zz} \ll 1$ for $T < T_m$ (Fig. 5) reveals that the NO_2^- anions rotate primarily about the c axis. When $T > T_m$, $(\Theta_{xx} + \Theta_{yy})/2\Theta_{zz} \simeq 1$, i.e., NaNO_2 becomes an orientational liquid.

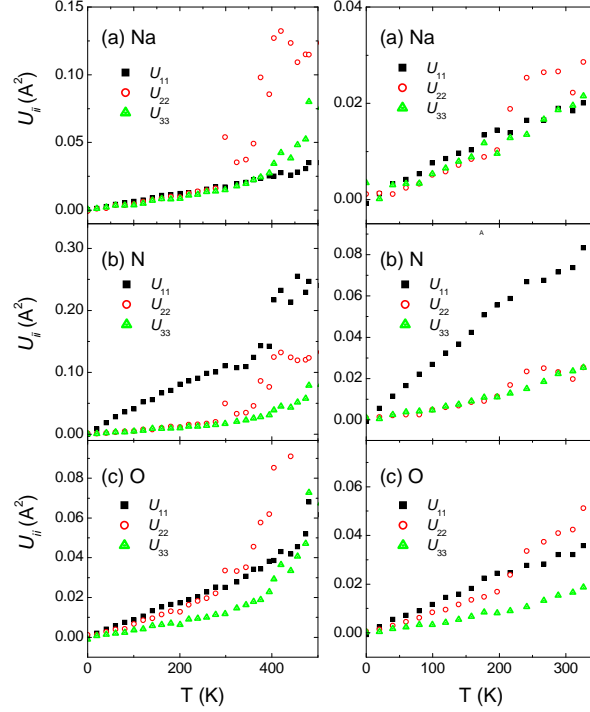


FIG. 6: Diagonal elements of the mean-square atomic displacements U_{ii} vs temperature. (a) Na, (b) N, and (c) O atom.

Further, in Fig. 6 we show the mean-square atomic displacements $U_{ii} = \langle u_i^2 \rangle$ where $i = 1, 2, 3$ denotes the displacements along the a, b, c axes, respectively. Different models of NO_2^- reversal are expected to satisfy the following conditions: (1) rotation around the c axis: $U_{22}(\text{N}), U_{33}(\text{N}) < U_{11}(\text{N})$ and $U_{22}(\text{O}), U_{33}(\text{O}) < U_{11}(\text{O})$; (2) rotation around the a axis: $U_{11}(\text{N}), U_{22}(\text{N}) < U_{33}(\text{N})$ and $U_{11}(\text{O}), U_{33}(\text{O}) < U_{22}(\text{O})$. This figure relates to recent X-ray experiments which used the same quantities to investigate the polarization reversal mechanism.^{4,5} The experiments confirmed that the first condition holds for both ferroelectric and paraelectric phases. Another important feature revealed by the experiments is that $U_{22}(\text{Na}), U_{33}(\text{Na}) < U_{11}(\text{Na})$ in the ferroelectric phase, whereas $U_{11}(\text{Na}), U_{33}(\text{Na}) < U_{22}(\text{Na})$ in the paraelectric phase. That is, $U_{11}(\text{Na})$ and $U_{22}(\text{Na})$ are reversed across T_C . These features are reproduced in Fig. 6 with exception of $U_{11}(\text{O}), U_{33}(\text{O}) < U_{22}(\text{O})$ in the paraelectric phase. This means the NO_2^- motions in our simulations are more mobile than those in the real crystal, rendering the simulated transition temperatures lower than the experimental values of $T_C \simeq 437$ K and the melting temperature 550 K. In other words, the barriers to NO_2^- rotation in our models are too small.

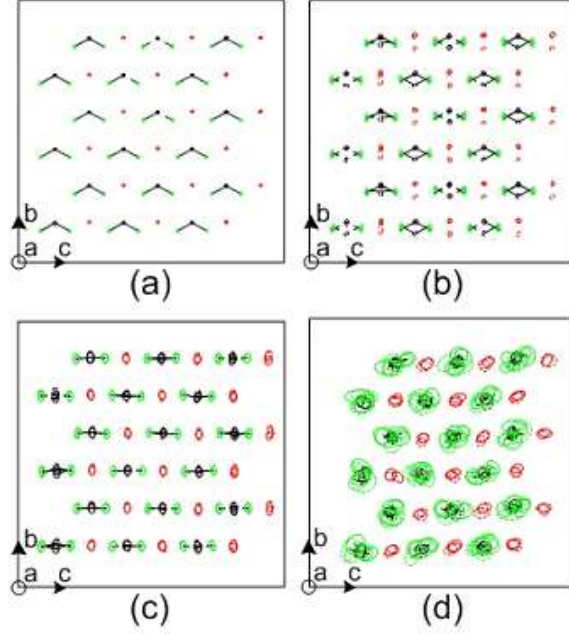


FIG. 7: Atomic positions of NaNO_2 viewed from the a direction obtained from the MD simulation for model I at (a) $T = 198$ K, (b) $T = 320$ K, (c) $T = 449$ K, and (d) $T = 535$ K.

In addition, in Fig. 7, we show the average crystal structures of NaNO_2 at different temperatures. The ellipsoids in these pictures represent the root-mean-square deviations of the atoms from their average positions and thus indicate the thermal motions of these atoms. The c -axis rotation mode can be clearly seen, particularly in Fig. 7(c).

According to the calculations described in the previous section, model II generally gives a better description of free NO_2^- and the intermolecular potential energies than model I. However, the simulation based on model I matches closer the experimental results than that based on model II, that is, T_C and T_m predicted by model I are closer to experiment, this indicates that the crystal fields and polarization effects are particularly important for quantitatively studying the NaNO_2 system, where the ferroelectric structure is considerably stabilized by anion polarization effects. Actually, the MPA employed by model I does not preserve the *ab initio* dipole moment of free NO_2^- . Rather, it overestimates the dipole moment by 120%, thus leading to higher NO_2^- rotational barriers than those predicted by model II, which in turn raises the transition temperature and provides a better simulation in comparison with the experiments.

It is worth mentioning the less desirable agreement between theoretical and experimental

volumes, namely, the 13% discrepancy for model I and 10% for model II. To address this we make one simple change: by following Waldman and Gordon,³⁹ we increase the kinetic energy term in the Gordon-Kim potentials by 5%, this reduces the discrepancy to 9% for model I and 6% for model II. Having done this we rerun the MD to obtain values of T_c of 360 K for model I and 303 K for model II. While this change worsens the value for model I, the value for model II is virtually unchanged. And in both cases the transition mechanism is unaltered. Thus the slight hardening of the short-range potentials removes most of the volume discrepancies. However, there is no material change in the mechanism of the phase transition. This robustness of the results with respect to minor variations in the potential demonstrates that our basic conclusion remain valid.

C. Rotational barriers

Based on the previous simulation results, the order-disorder phase transition in NaNO_2 involves the rotation of the nitrite ions. We devise a scheme to calculate the three rotational barriers for NO_2^- around the crystallographic a , b , and c axes with its center of mass fixed: we start from the experimental ferroelectric structure³⁵ as the ground state and calculate its energy difference with one of the two nitrite ions in the unit cell being rotated about the respective axis. The results are shown in Figs. 8(a) and 8(b). The bottom of each barrier, zero angle, is in the ferroelectric structure. For both models I and II, the rotation around the c -axis has an energy barrier 5-10 times smaller than those of the other rotations, which is a characteristic of nitrites.³¹ Hence, our calculations unambiguously reveal that the reorientation of NO_2^- in the paraelectric phase occur essentially by rotations around the c axis. In addition, the barriers calculated in model I are higher than that in model II, confirming that the transition temperature in model I will be higher than in model II.

In Figs. 8(c) and 8(d), we also plot the contribution to the rotational barriers purely from the electrostatic interaction, that is, in the point-charge model with the short range forces deleted. Comparing Fig. 8(a) with Fig. 8(c), or Fig. 8(b) with Fig. 8(d), we notice that the point-charge model gives rise to a quite different rotation barrier about the a axis: it bottoms at about $\pm 90^\circ$ and is lower than the ground state energy due to the omission of short-range interactions, which comes from overlap of the charge cloud of an atom with those of its neighbors.

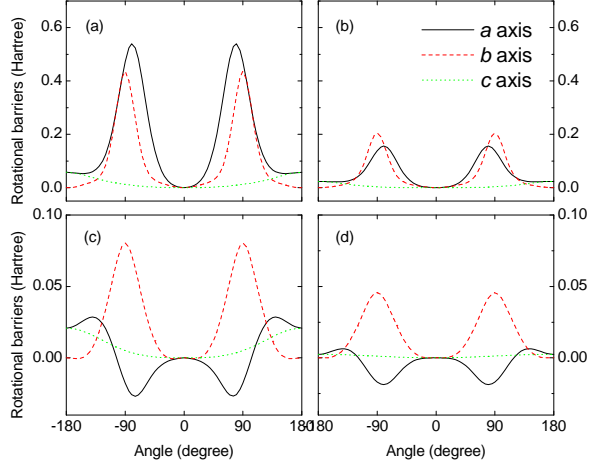


FIG. 8: Rotational barriers of one of the two nitrite ions in the unit cell around the a , b , and c axes with its center of mass fixed. (a)(b) for the GK model, (c)(d) for the point charge model. Left and right panels are for model I and II, respectively.

V. CRYSTAL-FIELD EFFECTS

In this section, we investigate the crystal-field effects on the NO_2^- ion, which include electrostatic interaction from the background lattice, overlap compression of the NO_2^- charge cloud through interaction with its neighbors, and charge-transfer between molecules which is usually small in ionic crystals. In the studies of monatomic ions²³ and cyanides⁴⁰, Fowler *et al.* showed that these effects could be successfully described by embedding the ion of interest, or a cluster consisting of the ion and its first shell of neighbors, into a lattice of point charges.

We therefore perform HF calculations based on the following two models.²³ First, the crystal field of ferroelectric NaNO_2 is simulated by placing the nitrite ion at the center of a $4 \times 4 \times 4$ orthorhombic point charge lattice with spacings equal to the experimental lattice parameters. Charges in the faces of the lattice are scaled to maintain overall neutrality. All anions except the central NO_2^- are represented by single point charges. Hence, there are 174 point charges surrounding the NO_2^- ion. Calculations of this type are referred to as CRYST. Obviously, in the CRYST calculation we take into account only the crystal-field effect arising purely from electrostatic interaction.

At the next level of sophistication, we replace the six nearest positive charges of the

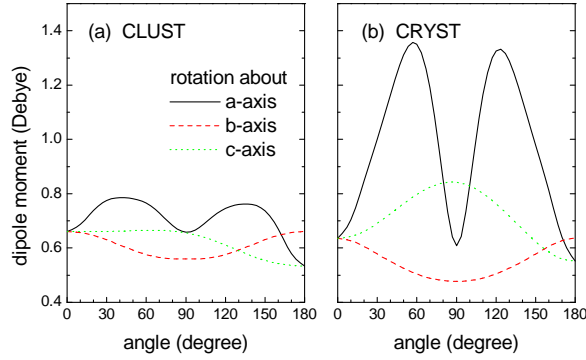


FIG. 9: Dipole moment of the central NO_2^- in a $4 \times 4 \times 4$ lattice as it rotates around the a, b, c axes through the center of its $(\text{Na}^+)_6$ cage. (a) CLUST and (b) CRYST.

central NO_2^- in the above lattice by the Na cations. Calculations of this type are referred to as CLUST. In both CRYST and CLUST calculations, the geometrical structure of the NO_2^- is fixed at its experimental values. We employ the same basis set, D95*, for the in-crystal NO_2^- ion as for the free NO_2^- ion. In order to keep the CLUST calculations to a manageable size, we use the minimal basis set, STO-3G, for the Na^+ ions unless specified. The cations, however, are relatively insensitive to the crystal environment and they are included here only to account for their compressing effect on the NO_2^- wave functions. We find that adding extra basis functions to Na^+ will not change the results significantly.

The in-crystal NO_2^- initially points in the b direction as in the ferroelectric phase of NaNO_2 ³⁵. Its dipole moment is 0.636 (CRYST) and 0.661 (CLUST) Debye, close to that in the free ion model, 0.661 Debye. Thus it appears that the crystal-field effect is small for this configuration. Subsequently, we rotate the NO_2^- about the a, b , and c axes and calculate the dipole moment of the rotated NO_2^- . The rotation center is taken to be the center of a $(\text{Na}^+)_6$ cage formed by the 6 neighboring sodium ions of the central NO_2^- ,⁶ (0, 0.279 Å, 0) in the coordinate convention of Fig. 1. The CLUST and CRYST results are depicted in Figs. 9(a) and 9(b), respectively. Clearly, the dipole moment of the NO_2^- changes considerably as it rotates, indicating strong crystal field effects on the reorientation of the NO_2^- . Since the electron density of the NO_2^- is compressed by its 6 neighboring sodium cations, the variation in magnitude of its dipole moment is smaller in the CLUST model than that in the CRYST model. The electron cloud of the NO_2^- is most and least variable when it rotates around the a and b axes, respectively; for the c -axis rotation, which has the lowest rotational barrier,

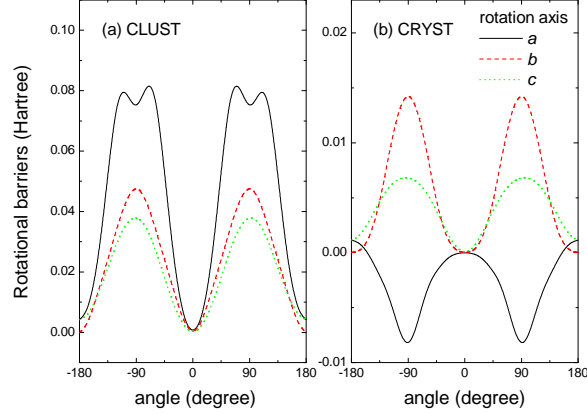


FIG. 10: *ab initio* barriers to rotation of the central NO_2^- in a $4 \times 4 \times 4$ lattice around the a , b , c axes through the center of its $(\text{Na}^+)_6$ cage. (a) CLUST and (b) CRYST.

the dipole moment goes down from 0.661 Debye at 0° to 0.534 Debye at 180° in the CLUST model, as shown Fig. 9(a).

In the context of population analysis, increase of the dipole moment of NO_2^- implies that more electrons are distributed on the O atom, i.e., electrons are flowing from the nitrogen atom to the oxygen atoms. Conversely, decrease of the dipole moment indicates a reversal in electron transfer. Therefore, we have demonstrated considerable *intramolecular* charge-transfer, although the intermolecular charge-transfer is usually small in ionic crystals. This intramolecular charge-transfer could be further elucidated based on the language of molecular orbitals (MOs): in the minimal basis set of atomic orbitals (AOs) on nitrogen and oxygen, each atom of the NO_2^- molecule contributes one p -orbital perpendicular to the molecular plane. Thus their linear combinations, which are determined by the crystal field, form three different π MOs extended over the entire molecule, thus leading to the above-mentioned intramolecular charge-transfer. Note that the mean HF polarizability of free NO_2^- , 14.156 in the atomic units, is much higher than that of free Na^+ , 0.343, calculated by using the 6-31* basis. Therefore, it is reasonable to expect that NO_2^- in solid NaNO_2 encountering different crystal-field environments as it rotates, redistributes its charge among the three constituent atoms to lower its energy.

In Fig. 10 we show that the rotational barriers of the central NO_2^- . On the whole, The CLUST results are similar to those in Figs. 8(a) and 8(b), while the CRYST results are similar to those in Figs. 8(c) and 8(d). The reason is that in the CRYST calculations we

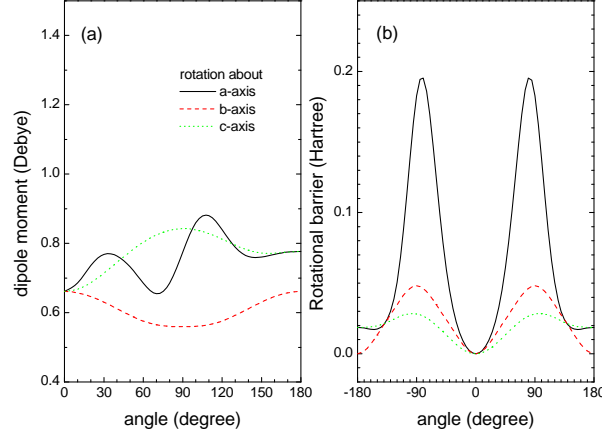


FIG. 11: In the CLUST model, NO_2^- rotates around the a, b, c axes through its center of mass. (a) dipole moment of NO_2^- , and (b) rotational barriers.

consider only the crystal-field effects originating purely from electrostatic interactions with the background point charges, similar to the point charge model used to obtain Figs. 8(c) and 8(d). Whereas, in the CLUST calculations, overlap compression is also taken into account, which is reflected in Figs. 8(a) and 8(b) as inclusion of short range repulsion. In Fig. 10(a), the barrier to the c -axis rotation is the lowest, but comparable with that to the b -axis rotation. This feature is caused by the fact that all background anions are represented by single point charges in our CLUST and CRYST calculations; however, we anticipate that restoring multipole moments of these background anions would increase the barrier difference among rotations about the a , b , and c axes.

To further elaborate the electronic polarization effect on NO_2^- arising from the crystal environment, we change the rotation center to the center of mass of the NO_2^- which was assumed in the model by Kremer and Siems.⁴¹ In this case, the dipole moment of NO_2^- and the rotational barriers are presented in Figs. 11(a) and 11(b), respectively. The dipole moment changes in a different way from that shown in Fig. 9(a). In particular, the dipole moment in the ferroelectric phase (0° -rotation) is larger than at 180° -rotation in Fig. 9(a), while it is smaller in Fig. 11(a). On the other hand, there is no qualitative discrepancy between Fig. 11(b) and Fig. 10(a); the main differences are: the rotational barrier about the a axis has risen by 135% while the barrier about the c axis is depressed by 26%. This means that the order of rotational barriers is enhanced by the change of the rotation center.

Although strong crystal field effects have been revealed by these *ab initio* calculations,

the rotational barriers obtained from the polarizable-ion models are in qualitative agreement with those from the rigid-ion models, confirming that the rigid-ion model is capable of describing the phase behavior in NaNO_2 .

VI. CONCLUDING REMARKS

We have presented MD simulations of NaNO_2 using a hybrid *a priori* method consisting of *ab initio* calculations and Gordon-Kim electron gas theory to analytically calculate the crystal potential surface. This method has been carefully examined by using different population analysis methods. We have carried out *ab initio* Hartree-Fock calculations of the intermolecular interactions for $\text{NO}_2^-:\text{Na}^+$ and $\text{NO}_2^-:\text{NO}_2^-$ dimers and concluded that the pair potentials of the rigid-ion model can correctly reproduce the *ab initio* results. We demonstrated that a rigid-ion model is capable of describing phase behavior in solid NaNO_2 .

The crystal-field effects on the NO_2^- ion are also addressed in two polarizable-ion models for which the ferroelectric phase of NaNO_2 was found to have a larger dipole moment of NO_2^- than the 180° -rotation phase. Remarkable internal charge-transfer effect is found to be stabilizing the crystal structure of NaNO_2 . In our MD simulations, two rigid-ion models using MPA and FPA, respectively, have been studied. The one using MPA, which overestimates the dipole moment of NO_2^- , gives rise to the more comparable results with the experiments, since such overestimation also stabilizes the crystal structure, thus mimics the anion polarization effect. To quantitatively simulate NaNO_2 , a more elaborate polarizable-ion model is needed.

Acknowledgments

Helpful discussions with Dr. L. L. Boyer are gratefully acknowledged. This work was supposed by the Nebraska Research Initiative, the Nebraska EPSCoR-NSF Grant EPS-9720643, and Department of the Army Grants DAAG 55-98-1-0273 and DAAG 55-99-1-0106. W. N. M. is grateful for the support from the Office of Naval Research.

* Electronic address: wgyin@yahoo.com

- ¹ S. Sawada, S. Nomura, S. Fujii, and I. Yoshida, Phys. Rev. Lett. **1**, 320 (1958).
- ² M. E. Lines and A. M. Glass, *Principles and Applications of Ferroelectrics and Related Materials* (Clarendon, Oxford, 1977).
- ³ A. V. Fokin, Y. A. Kumzerov, N. M. Okuneva, A. A. Naberezhnov, S. B. Vakhrushev, I. V. Golosovsky, and A. I. Kurbakov, Phys. Rev. Lett. **89**, 175503 (2002).
- ⁴ T. Gohda, M. Ichikawa, T. Gustafsson, and I. Olovsson, Phys. Rev. B **63**, 014101 (2000).
- ⁵ K. Komatsu, K. Itoh, and E. Nakamura, J. Phys. Soc. Japan **57**, 2836 (1988).
- ⁶ K. D. Ehrhardt and K. H. Michel, Phys. Rev. Lett. **46**, 291 (1981).
- ⁷ W. Kinase and K. Takahashi, J. Phys. Soc. Japan **61**, 329 (1992).
- ⁸ M. L. Klein, I. R. McDonald, and Y. Ozaki, Phys. Rev. Lett. **48**, 1197 (1982).
- ⁹ M. L. Klein and I. R. McDonald, Proc. R. Soc. Lond. **A382**, 471 (1982).
- ¹⁰ R. M. Lynden-bell, R. W. Impey, and M. L. Klein, Chem. Phys. **109**, 25 (1986).
- ¹¹ H. M. Lu and J. R. Hardy, Solid State Commun. **87**, 1151 (1993).
- ¹² H. M. Lu and J. R. Hardy, Phys. Rev. Lett. **64**, 661 (1990).
- ¹³ P. J. Edwardson, L. L. Boyer, R. L. Newman, D. H. Fox, J. R. Hardy, J. W. Flocken, R. A. Guenther, and W. Mei, Phys. Rev. B **39**, 9738 (1989).
- ¹⁴ H. M. Lu and J. R. Hardy, Phys. Rev. B **42**, 8339 (1990).
- ¹⁵ J. Liu, C. Duan, W. N. Mei, R. W. Smith, and J. R. Hardy, J. Solid State Chem. **163**, 294 (2002).
- ¹⁶ D. Liu, H. M. Lu, F. G. Ullman, and J. R. Hardy, Phys. Rev. B **43**, 6202 (1991).
- ¹⁷ J. Liu, C. Duan, W. N. Mei, R. W. Smith, and J. R. Hardy, J. Chem. Phys. **116**, 3864 (2002).
- ¹⁸ H. M. Lu and J. R. Hardy, Phys. Rev. B **44**, 7215 (1991).
- ¹⁹ J. Liu, C. Duan, M. M. Ossowski, W. N. Mei, R. W. Smith, and J. R. Hardy, J. Solid State Chem. **160**, 222 (2001).
- ²⁰ J. Liu, C. Duan, M. M. Ossowski, W. N. Mei, R. W. Smith, and J. R. Hardy, J. Phys. Chem. Solids **63**, 409 (2002).
- ²¹ W. Hehre, L. Radom, P. Schleyer, and J. Pople, *Ab initio molecular orbital theory* (John Wiley & Sons, New York, 1986), p. 336.
- ²² P. Ravindran, A. Delin, B. Johansson, O. Eriksson, and J. M. Wills, Phys. Rev. B **59**, 1776 (1999).
- ²³ P. W. Fowler and P. A. Madden, Phys. Rev. B **29**, 1035 (1984).

- ²⁴ Y. S. Kim and R. G. Gordon, Phys. Rev. B **9**, 3548 (1974).
- ²⁵ A. J. Cohen and R. G. Gordon, Phys. Rev. B **12**, 3228 (1975).
- ²⁶ L. L. Boyer, Phys. Rev. Lett. **42**, 584 (1979).
- ²⁷ M. Sepiarsky, S. R. Phillpot, D. Wolf, M. G. Stachiotti, and R. L. Migoni, Appl. Phys. Lett. **76**, 3986 (2000).
- ²⁸ M. J. F. *et al.*, *GAUSSIAN 98, Revision A.11.3* (Gaussian, Inc., Pittsburgh PA, 2002).
- ²⁹ R. G. Gordon and Y. S. Kim, J. Chem. Phys. **56**, 3122 (1972).
- ³⁰ M. Waldman and R. G. Gordon, J. Chem. Phys. **71**, 1340 (1979).
- ³¹ C. G. Duan, W. N. Mei, R. W. Smith, J. Liu, M. M. Ossowski, and J. R. Hardy, Phys. Rev. B **63**, 144105 (2001).
- ³² G. A. Parker, R. L. Snow, and R. T. Pack, Chem. Phys. Lett. **33**, 399 (1975).
- ³³ A. Banerjee, R. Shepard, and J. Simons, J. Chem. Phys. **73**, 1814 (1980).
- ³⁴ E. Clementi and C. Roetti, At. Data Nucl. Data Tables **14**, 177 (1974).
- ³⁵ M. I. Kay, Ferroelectrics **4**, 235 (1972).
- ³⁶ C. M. Hartwig, E. Wiener-Avnear, and S. P. S. Porto, Phys. Rev. B **5**, 79 (1972).
- ³⁷ M. Okuda, S. Ohba, Y. Saito, T. Ito, and I. Shibuya, Acta Cryst. B **46**, 343 (1990).
- ³⁸ M. Parrinello and A. Rahman, Phys. Rev. Lett. **45**, 1196 (1980).
- ³⁹ M. Waldman and R. G. Gordon, J. Chem. Phys. **71**, 1325 (1979).
- ⁴⁰ P. W. Fowler and M. L. Klein, J. Chem. Phys. **85**, 3913 (1986).
- ⁴¹ J. W. Kremer and R. Siems, Ferroelectrics **79**, 35 (1988).